9-2018

Removal of Cu2+ and Ni2+ from Aqueous Solution using SnO2 Nanomaterial effect of: pH, Time, Temperature, interfering cations

Abigail M. Zepeda
The University of Texas Rio Grande Valley

Daisy Gonzalez
The University of Texas Rio Grande Valley

Luis Gonzalez Heredia

Karina Marquez
The University of Texas Rio Grande Valley

Cesar Perez
The University of Texas Rio Grande Valley

See next page for additional authors

Recommended Citation

Zepeda, Abigail M., Daisy Gonzalez, Luis Gonzalez Heredia, Karina Marquez, Cesar Perez, Erika Pena, K. Flores, et al. 2018. "Removal of Cu2+ and Ni2+ from Aqueous Solution Using SnO2 Nanomaterial Effect of: PH, Time, Temperature, Interfering Cations." Microchemical Journal 141 (September): 188–96. https://doi.org/10.1016/j.microc.2018.05.020.

HHS Public Access

Author manuscript

Microchem J. Author manuscript; available in PMC 2019 September 01.

Published in final edited form as:

Microchem J. 2018 September ; 141: 188–196. doi:10.1016/j.microc.2018.05.020.

Removal of Cu^{2+} and Ni^{2+} from Aqueous Solution using SnO_2 Nanomaterial effect of: pH, Time, Temperature, interfering cations

Abigail M. Zepeda[a], **Daisy Gonzalez**[a], **Luis Gonzalez Heredia**[a], **Karina Marquez**[a], **Cesar Perez**[a], **Erika Pena**[a], **K. Flores**[a], **C. Valdes**[a], **T. M. Eubanks**[a], **J.G. Parsons**[a,b,*], and **J. Cantu**

[a]Department of Chemistry University of Texas Rio Grande Valley, One West University Blvd. Brownsville TX 78521

[b]School of Earth, Environmental, and Marine Sciences University of Texas Rio Grande Valley, One West University Blvd. Brownsville TX 78521

Abstract

Tin oxide, SnO_2, nanomaterial was synthesized and tested for the removal of Cu^{2+} and Ni^{2+} ions from aqueous solutions. Various parameters for the binding were investigated in batch studied, which included pH, time, temperature, and interferences. In addition, isotherm studied were performed to determine the maximum binding capacity for both Cu^{2+} and Ni^{2+} ions. The optimal binding pH determined from the effects of pH were to be at pH 5 for both the Cu^{2+} and Ni^{2+} ions. The isotherm studies were performed at temperatures of 4°C, 25 °C, and 45 °C for both the Cu^{2+} and Ni^{2+} ions and were found to follow the Langmuir isotherm model. The binding capacities for the Cu^{2+} ions were 2.63 mg/g, 2.95 mg/g and 3.27 mg/g at the aforementioned temperatures, respectively. Whereas the binding capacities for Ni^{2+} were 0.79 mg/g, 1.07 mg/g, and 1.46 mg/g at the respective temperatures. The determined thermodynamic parameters for the binding showed that the binding processes for the reactions were endothermic, as the ΔG was observed to decrease with decreasing temperatures. As well the ΔH was 28.73 kJ/mol for Cu^{2+} (III) and 13.37 kJ/mol for Ni^{2+}. The ΔS was observed to be 92.65 J/mol for Cu^{2+} and 54.53 J/mol for Ni^{2+}. The free energy of adsorption for the Cu^{2+} was determined to be 13.99 kJ/mol and the activation energy for the binding of Ni^{2+} was determined to be 8.09 KJ/mol. The activation energy data indicate that the reaction was occurring through chemisorption

Keywords

Copper; Nickel; Adsorption; SnO_2; thermodynamics

*Corresponding author: Tel.:+1 956 882 7772, jason.parsons@utrgv.edu.

1.0 Introduction

Heavy metal ions, such as nickel Ni^{2+} and copper Cu^{2+}, are found in discharged wastewaters from the industries, dissolution/weathering of natural minerals, and runoff from residential areas. Industrialization of the world has been one of the main reason for heavy metals in wastewaters. Industrial processes that commonly discharge Ni^{2+} and Cu^{2+} into wastewaters include: metal plating facilities, metal finishing, chemical, fertilizer, paperboard mills, etc. [1–6] Heavy metals are also incorporated into natural waters, through natural mineral dissolution. [7] Residential areas discharge different concentrations for both Ni^{2+} and Cu^{2+} into wastewaters through the use of various household products. [8] Therefore, Cu^{2+} and Ni^{2+} in water has become a concern. Removing these pollutants from the water has become an important process with the increasing amount of industrial activities. [9] There are negative effects of Ni^{2+} and Cu^{2+} in the wastewaters; that affect both environmental and human health. [10]

Negative health effects presented by Ni^{2+} and Cu^{2+}, along with other heavy metals from wastewater has become a concern to both environmental and human health. [2, 6, 10–12] Increasing concern with environmental contaminants has raised attention to heavy metals as potential hazards in the environment. The acceptable maximum limit concentration for Ni^{2+} and Cu^{2+} present in water is 1.0 mg/L [1]. Certain industries that release these wastewaters into the environment have reported a Ni^{2+} and Cu^{2+} concentrations that range from 2.0 mg/L to 900 mg/L [3]. With high concentrations of Ni^{2+} and Cu^{2+} water, the aquatic and plant ecosystem are first to be affected. Since Ni^{2+} and Cu^{2+} have a high solubility, theses metals are easily absorbed at high concentrations. The accumulated Ni^{2+} and Cu^{2+} will eventually make way into the food industry [4]. Heavy metals are non-biodegradable, the accumulation of Ni and Cu from the aquatic and plant organisms are eventually ingested and biomagnified in the food web. The ingestion of high concentrations of Ni^{2+} and Cu^{2+} can cause various diseases and disorders to the human body. [6, 13] Cu^{2+} is known to be beneficial for metabolism however, ingestion of excess amount is known to be toxic. [13] Cu^{2+} has been linked to liver damage, Wilson disease, kidney failure, lung cancer, and insomnia. [4, 6, 12,] Ni^{2+} in small doses is non-toxic towards humans, but ingestion of high concentrations is toxic and can causes problems such as skin dermatitis, nausea, chronic asthma, coughing, and cancer. [4, 6, 12, 13]

There are various methods that allow for removal of heavy metals from water, including adsorption, electrochemical treatments, ion exchange and chemical precipitation, and others. [8,14–17] Several methods are available for removal of nickel, such as alkaline chemical precipitation by lime addition, adsorption, ion-exchange process, evaporative recovery method, and reverse osmosis. [18] Treatment of water contaminated metal ions using adsorption has shown to be one of the most efficient methods. [20–21]. However, many that are mentioned suffer due to high cost and non-specific for particular ions or groups of ions. [18,20,22]. Recent studies have shown adsorption to be one of the most efficient methods for removal of heavy metals, specifically copper ions, from waste waters due to its ease of employment. [8, 14] Adsorbents are typically cost-effective and include activated carbons, zeolites, carbon nanotubes, and Nano-materials. [8, 14, 15] Nanomaterials are promising adsorbents because of their larger surface area, high number of active sites, and low

diffusion resistance. [8, 14] Nanomaterials make particularly good adsorbents for heavy metal removal from wastewaters. It has been shown that these materials have high selectivity and large surface area, resulting in high capacity, which adds to their efficiency. [19]

For example, metal oxides such as MgO, Fe_2O_3, ZnO, TiO_2, and MnO_2 can be used to remove metal ions from aqueous solution. Transition metal oxides are generally non-toxic and are low-cost. [16, 17] More specifically, Fe_3O_4 and Fe_2O_3 nanoparticles have shown much promise in the removal of As(III)/As(V), Cr(III)/Cr(VI), Pb(II), Cu(II), and Se(IV)/Se(VI) [24–27]. The binding of As(III)/(VI) has shown to have binding capacities in the range of thousands of mg/g. Whereas the binding of Cr(VI) and Cr(III) have shown binding capacities in the range of 5 to 16 mg/g. Further studies have shown that iron based nanomaterials have shown binding capacities of 37 mg/g and 166 mg/g on the higher end for Cu(II) and Pb(II), respectively. Alternatively, Mn-Oxide based nanomaterials have also shown much promise in the remediation/removal of metals from aqueous solution [24–27]

In the present study SnO_2 nanoparticles were synthesized and tested for the ability to remove Cu^{2+} and Ni^{2+} ions from aqueous solution. The nanoparticles were synthesized using an aqueous sol-gel method followed by thermal treatment. X-ray diffraction confirmed the synthesis of the SnO_2 nanoparticles, with an average grain size of 11.34 ± 0.58 nm, as determined using Scherer's equation. Studies were performed to determine the effects of pH, time, and hard cations on the binding of Cu^{2+} and Ni^{2+} to the SnO_2 nanomaterial. Further studies were performed to determine the binding capacity, thermodynamics, and activation energy for the binding of the Cu^{2+} and Ni^{2+} ions to the synthetic SnO_2 nanomaterial.

2.0 Experimental

2.1 Synthesis of SnO_2 Nanoparticles

The SnO_2 nanoparticles were prepared through a precipitation method. A 30 mmol solution consisting of $SnCl_4$ $5H_2O$ was prepared using 10.5171 g of $SnCl_4{\cdot}5H_2O$ dissolved in deionized water (18 MΩ). An aliquot of a 120 mmol solution of NaOH was then slowly titrated into the SnO_2 solution. After titration the $SnCl_4$–NaOH solution was filtered and the precipitate was air dried. Subsequent to drying the precipitate was placed in an alumina crucible then heated in a muffle furnace to 650°C, held constant for 2 hours, and cooled to room temperature.

2.2 XRD Characterization of SnO_2 Nanoparticles

X-Ray powder diffraction analysis was performed using a Rigaku MiniFlex II X-ray Diffractometer. The operating parameters of the XRD were as follows: a 0.05° step in 2θ, a 5-second counting time, a copper source operating at 30 kV and 15 mA using the K_α 1.54 Å, a nickel filter, and a scintillation detector, and the data was collected from 20–60 in 2θ. After the diffraction pattern was collected it was extracted and analyzed using the FullProf software. The diffraction data was fitted using the LeBail fitting procedure, within the FullProf software, and crystallographic data from the literature [28–30].

2.3 SEM Characterization of SnO_2 Nanoparticles

SEM characterization was performed using a Zeiss LS10 electron microscope. The data were collected using an operating voltage of 28.33 keV, and a working distance of 5.5 mm.

2.4 pH Profile

300 ppb solutions were prepared for both Cu^{2+} and Ni^{2+} from their respective nitrate salts. The Cu^{2+} and Ni^{2+}solutions were then pH adjusted to pHs of 2, 3, 4, 5, and 6 using either dilute HNO_3 or dilute NaOH solutions. At each pH, 4.0 mL aliquots were transferred into clean 5 mL test tubes containing 10 mg of the SnO_2 nanomaterial. In addition, control samples were prepared, which consisted of only the pH adjusted metal ion solution. All reaction samples and control samples were repeated in triplicate, and treated in the same, for statistical and quality control purposes. The tubes containing the reaction and control samples were equilibrated for 1 hr. Subsequent, to equilibration, the reaction and control samples were centrifuged at 3,200 RPM for 5 min. The supernatants were decanted and transferred into clean 5 mL test tubes and stored for further analysis. The reaction and control samples were analyzed using a Perkin Elmer Optima 8300 inductively coupled plasma optical emission spectrometer (ICP-OES) all calibration curves produced correlation coefficients (R^2) of 0.99 or better.

2.5 Capacity Studies

The Cu^{2+} and Ni^{2+} binding capacities to the SnO_2 nanomaterial were determined using isotherm studies. Samples consisting of 10 mg of the SnO_2 nanomaterial were added to clean 5 mL tubes and 4.0 mL aliquots of either Cu^{2+} or Ni^{2+} at concentrations of 0.3, 3, 30, 300, and 1000 ppm were added. The Cu^{2+} and Ni^{2+} solutions were previously adjusted to a pH of 5, which was determined to be the optimum binding pH from the pH studies. Furthermore, control samples consisting of either Cu^{2+} or Ni^{2+} solutions, in the absence of the nanomaterial were prepared and treated in the same manner as the samples The reaction samples and control samples were capped and equilibrated on a rock for 1 hr. Subsequent to equilibration the reaction and control samples were centrifuged at 3200 RPM for 5 min. The supernatants were decanted into clean tubes and saved for further analysis. All reaction and control samples performed in triplicate for statistical quality assurance and control purposes. The reaction and control samples were analyzed for metal content using a Perkin Elmer optima 8300 ICP-OES. In addition, all calibration curved used in the study had correlation coefficients (R^2) of 0.99 or better.

2.6 Thermodynamic Studies

The thermodynamics studies were performed the same as the isotherm studies; however the temperatures of the reactions were performed at 4°C, 25°C, and 45°C. 4.0 mL aliquots of pH adjusted of either Cu^{2+} or Ni^{2+} solutions at concentrations of 0.3, 3, 30, 100, 300, and 1000 ppm solutions were added to 5.0 mL test tubes containing 10 mg of the SnO_2 nanomaterial. Furthermore, control samples consisting of either Cu^{2+} or Ni^{2+} solutions, in the absence of the nanomaterial were prepared and treated in the same manner as the samples The reaction samples and control samples were capped and equilibrated on a rock for 1 hr. Subsequent to equilibration the reaction and control samples were centrifuged at 3,200 RPM for 5 min. The

supernatants were decanted intro clean tubes and saved for further analysis. All reaction and control samples performed in triplicate for statistical quality assurance and control purposes. The reaction and control samples were analyzed for metal content using a Perkin Elmer optima 8300 ICP-OES. In addition, all calibration curved used in the study had correlation coefficients (R^2) of 0.99 or better.

2.7 Kinetic Studies

30 ppm solutions of Cu^{2+} and Ni^{2+} were prepared and adjusted to the optimum binding pH using dilute nitric acid or sodium hydroxide. 4.0 mL aliquots of either the pH adjusted Cu^{2+} or Ni^{2+} were added into 5.0 mL tubes, which contained 10 mg of the SnO_2 nanomaterial. In addition, control samples consisting of the metal ion only in solution were prepared and treated the same as the reaction samples. The reaction and control samples were equilibrated at temperatures of either 4 °C, 25 °C, or 45 °C at various times. The reaction and control samples were equilibrated in triplicate for reaction times of 5, 10, 15, 30, 60, 90, and 120 minutes. This procedure was repeated for each ion at each temperature. Subsequent to equilibration the samples were centrifuged for 5 minutes at 3,200 RPM and the supernatants were decanted and saved for further analysis. The reaction and control samples were analyzed for metal content using a Perkin Elmer optima 8300 ICP-OES. In addition, all calibration curves used in the study had correlation coefficients (R^2) of 0.99 or better.

2.8 Interference Studies

Studies were performed to investigate the effects of hard cations on the binding of Cu^{2+} and Ni^{2+} to the SnO_2 nanomaterial. The investigated were Ca^{2+}, K^+, Mg^{2+}, and Na^+. Solution consisting of the individual cations were prepared at pH 5 (the optimum binding pH) the following concentrations 0.3, 3, 30, 100, 300, and 1000 ppm with a Cu^{2+} or Ni^{2+} concentration of 300 ppb. In addition, a combined interference solution was prepared that contained each of the cations, at the aforementioned concentrations, of either Cu^{2+} or Ni^{2+} at 300 ppb. The combined interference solution consisted of 0.3, 3, 30, 100, 300, and 1000 ppm. 4.0 mL aliquots of the pH adjusted solutions were added to the tubes containing 10 mg of SnO_2. Furthermore, control samples consisting of either Cu^{2+} or Ni^{2+} solutions, in the absence of the nanomaterial were prepared and treated in the same manner as the samples. The reaction samples and control samples were capped and equilibrated for 1 hr. Subsequent to equilibration the reaction and control samples were centrifuged at 3200 RPM for 5 min. The supernatants were decanted intro clean tubes and saved for further analysis. All reaction and control samples performed in triplicate for statistical quality assurance and control purposes. The reaction and control samples were analyzed for metal content using a Perkin Elmer optima 8300 ICP-OES. All calibration curves used in the study had correlation coefficients (R^2) of 0.99 or better.

2.9 GFAAS Analysis Parameters

A Perkin Elmer PinAAcle 900 operated in Graphite Furnace mode was used to collect the interference portion of the data. The operating parameters of the GFAAS for the analysis of the copper and nickel binding are presented in Table 1 and Table 2, respectively.

2.10 ICP-OES Analysis

A Perkin Elmer Optima 8300 DV ICP-OES was used for data collection as mentioned earlier. The operating parameters for the collection of the copper and nickel data using the ICP-OES are shown in Table 3.

3.0 Results and Discussion

3.1 X-Ray diffraction analysis

Figure 1 shows the powder x-ray diffraction pattern, and the LeBail fitting of the synthesized SnO_2 nanomaterial. As can be seen in Figure 1, only a small residual can be observed between the data and the fitting. The fitting had final χ^2 of 0.815 indicating an excellent agreement between the data and the crystal structure of SnO_2, as shown in the fitting results present in Table 4. From the data the following Bragg peaks, with the 2θ positions given in parentheses, were observed: 110 (26.621), 101 (33.924), 200 (38.003), 111 (39.034), 210 (42.695), 211 (51.847), 220 (54.833), 002 (57.918), 310 (61.969), 221 (62.694), 112 (64.842), 301 (66.062), and 311 (69.345). The observed peaks are consistent with the SnO_2 crystal structure at the associated 2θ positions, furthermore no extra peaks were observed, no peaks were missing from the diffraction pattern. The XRD data indicating the synthesized nanomaterial SnO_2 in the P42/mnm (tetragonal) crystal structure with a=b= 4.7371 Å and c=3.1854 Å [30]. In addition, the peaks observed in the diffraction pattern are relatively broad with low intensity, which indicates a small crystallite size present in the sample. Further analysis using Scherer's equation (shown below):

$$d = \frac{0.9\lambda}{B\left(cos\frac{2\theta}{2}\right)}$$

Where 0.9 is a correction factor used for the determination of the full width half maximum (FWHM), λ is the wavelength of the copper source 1.54 Å, B is the FWHM of the diffraction peak, and $\cos\frac{2\theta}{2}$ is the cosine of the angle where the diffraction peak was observed. The analysis of the diffraction based on three different peaks the average grain size of the material was 11.22 nm ± 0.58 nm. The diffraction data indicates that the synthesized material was a SnO_2 crystal in the nanometer size range.

SEM—Figure 2 shows the SEM image of the synthesized SnO_2 nanomaterial. The material consists of a particles with an approximate size of 100 nm. However, upon closer inspection the particle are clusters of very small particles with approximate sizes of 10–20 nm. Confirming the data determined from the XRD analysis that the Synthesized SnO_2 was nanoparticles.

3.2 pH Studies

The effect of pH on the binding of Ni^{2+} and Cu^{2+} to the SnO_2 nanomaterial from pH 2 through 6 are shown in Fig. 3. As can be seen in Fig. 3 the binding of both the Cu^{2+} and Ni^{2+} was very low at pH 2. The binding was observed to increase at pH 3 for Cu^{2+} a binding of approximately 45% was observed. Whereas the binding of Ni^{2+} was observed to bind

between 5 and 10%. However, binding of both Cu^{2+} and Ni^{2+} was observed to increase at pH 4, 5, and 6 to approximately 90–100% at their respective highest binding pH. The low binding at low pH has been observed with many metal cations and is generally attributed to surface charge of the binding material [24–28, 31–33]. At pH's below the zero point charge a particle surface becomes positively charged and effective repels the cations in solution from binding. At pH around the Zero point charge the surface has a neutral charge. Whereas at pH's above the Zero point charge the nanomaterial has a negative charge and attracts the metal ions facilitating the binding. For SnO_2 it has been determined in the literature that the pH of zero point charge varies from 3.5 to 4.0 [31, 32]. The large increase in binding for both the Cu^{2+} and Ni^{2+} between pH 3 and pH 4 is supported by the data in the literature show the pZc of SnO_2 ranges between 3.5–4.0, the surface becomes negatively charged between pH 3 and 4 and an increase in the binding occurs. Similarly, increase in the binding of Cu^{2+} and Ni^{2+} are observed when binding to redmud, magnetic particles with alginate, activated carbon, and alumina nanomaterials [34–37]. The binding of metal ions is not only controlled by the surface charge there are other effects that are observed to either influence the binding or control binding, which include photo-chemical reactions and redox reactions oxidative or reductive dissolution of the material [33]. The observed decrease in the copper binding, between pH 4 and pH 6 could be a conversion of the SnO_2 to a hydrous form which may be less reactive towards the Cu^{2+} ions in solution. There are many different factors at work in the reaction solution including redox coupling and the formation of metal hydroxides. For example, the formation of $Cu(OH)_2$ the K_{sp} is 1.6×10^{-19}, and the K_{sp} for $Ni(OH)_2$ is 1.6×10^{-16} [9]. Copper and nickel have 4 orders of magnitude in the difference between the solubility constants for the hydroxide, so $Cu(OH)_2$ will form at a lower pH than $Cu(OH)_2$, which would result in lower percentage binding of the Cu^{2+} than the Ni^{2+} due to precipitation of the metal ions. This could also be coupled with redox-chemistry, SnO^2 is a photo active material capable of reducing and oxidizing materials in solution. Ni^{2+} reduction has a potential of −0.23V and Cu^{2+} has a potential of +0.16 V, which means that Ni^{2+} is more easily reduced than is copper, so there may be a precipitation of the Ni^{2+} on the surface of the SnO_2, which would be observed as an increase in the binding.

3.3 Capacity Studies

The capacity data for the binding of Ni^{2+} and Cu^{2+} to the SnO_2 nanomaterial are presented in Table 4. The Langmuir isotherm had the best fitting of the data or the highest correlation coefficients. In addition, the reactions were performed using temperatures of 4° C, 21° C, and 45° C. The data show an increasing trend in the binding capacity with increasing temperature of reaction, for both the Cu^{2+} and Ni^{2+} cations in solution. The increase in binding with increasing temperature indicates an endothermic reaction is occurring for the binding of both Cu^{2+} and Ni^{2+} ions to the SnO_2 nanomaterial. Increases in binding capacity with increasing temperature have been observed in the reaction binding of either Cu^{2+} and/or Ni^{2+} to Kalonite, Iron oxide coated sand, magnetic nanoparticles impregnated onto tea waste, and chitosan/clay/magnetie composite materials [9, 38, 39, 40]. However, the room temperature binding capacity observed for the SnO_2 with Cu^{2+} (2.95 mg/g or 0.463 mmol/g) and Ni^{2+} (1.08 mg/g or 0.018 mmol/g), are observed to be within the range observed for the binding of Cu^{2+} and Ni^{2+} reported in the literature to numerous nanomaterials as shown in Table 5. The values for the present study fall around the mean

values in the literature. The increase in binding with increasing temperature can be attributed to a number of different chemical factors. The release of H^+ from the surface of the nanomaterial will occur easier at higher temperature. The correlation between the binding capacities and the temperature increase have been linked to possible changes in the size of the pores of the nanomaterial absorbent as well as the increase in the number of absorbent sites, which is the result of breaking bonds near the edge of the particles at 45° C [2]. Furthermore, the collisions occurring between the dissolved metal ions and the nanoparticle surface will occur at a higher frequency, and may result in a higher binding capacity. The results from the binding capacity study showing increasing binding with increasing temperature indicates that the binging occurs through an endothermic process.

3.4 Kinetics

Table 6 shows the kinetics data obtained for binding of Cu^{2+} and Ni^{2+} to the SnO_2 nanomaterial at temperatures of 4, 21, and 45 °C and the associated correlation coefficients (R^2) for the fittings. The data was found to fit well to a zeroth order kinetics model, all fittings had correlation coefficients fell within the 0.99 to 0.98 range indicating a good fit between the data and the model. The zeroth order kinetics model has been found be effective in fitting many adsorption studies [53,54]. However, in studies where diffusion into pores within the structure is observed the second order kinetic models and diffusion models are found to be more suitable. At lower temperatures Cu^{2+} was found to bind at higher rates compared to the Ni^{2+} ions. However, the rate of the Ni^{2+} ions was observed to be higher at the 45°C. In addition, the rate of the reaction was observed to increase with increasing temperature indicating that the reaction was endothermic in nature.

3.5 Thermodynamics Studies

Activation energy is an important reaction parameter as are the thermodynamic parameters, which helps to determine the type of reaction occurring. In the present study Arrhenius plots were used to determine the Activation energy for the binding of Cu^{2+} and Ni^{2+} to the SnO_2 nanomaterial. The plots are based on the Arrhenius equation shown in equation (1) below:

$$lnK = \ln(A) - \frac{E_a}{RT} \quad (1)$$

Where ln(k) is the natural log of the rate constant, ln(A) is the frequency factor, E_a is the activation energy for the reaction, R is the gas constant, T is the temperature in Kelvin. By plotting the ln(k) against 1/T the Arrhenius plot is developed. The slope of the line is the negative of the activation energy divided by the gas constant. The Arrhenius plots are shown in Figure 4 and the calculated E_a for the reaction are presented in Table 6. Activation energy gives an indication of the type of reaction that is occurring between the metal ion and the adsorbent in solution. In general activation energies around 4.0 kJ/mol indicate that physisorption is the main mechanism for the binding process [53]. Whereas, activation energies above 4.0 kJ/mol are indicative of a chemisorption process [53]. In the present study the activation energies are well above 4.0 kJ/mol, which indicates that both the Cu^{2+} and Ni^{2+} ions are binding through chemisorption to the SnO_2 nanomaterial. The small

difference between the activation energies of approximately 6 kJ/mol can be attributed to the differences in affinity of the metal ions to the sorbent.

The thermodynamic data presented in Table 6 in addition to the E_a includes the Gibbs free energy (ΔG), enthalpy (ΔH), and entropy (ΔS). The thermodynamic plot for the determination of the ΔH and ΔS of binding is shown in Figure 5. The ΔG of binding for the Cu^{2+} and Ni^{2+} were calculated based on the relationship of distribution coefficient of the ions between the SnO_2 and aqueous solution. The values were determined from the data collected at three temperatures and the respective slopes of the linearized Langmuir Isotherms. The slope of the linear form of the Langmuir equation is the inverse of the distribution coefficient. The relationship between K_d and ΔG is shown in the following equation (2):

$$\Delta G = -RTLnk_d \quad (2)$$

ΔG is the calculated change in Gibbs free energy, R is the gas constant (8.314 J/$Mol^{-1}K^{-1}$), and T is the reaction temperature in Kelvin. The observed trend for the ΔG for the Cu^{2+} and Ni^{2+} ions to the SnO_2 nanomaterial was a decrease in the value with an increase in temperature. The data indicate that the binding is endothermic, the binding process becomes more spontaneous as temperature was increased. In addition, it has been shown in the literature that ΔG values below 18 kJ/mol (with respect to the absolute value) are indicative of an adsorption reaction dominated by physisorption [53]. The ΔG sorption for copper and nickel ions has been studied for different metal oxides. The thermodynamics for the adsorption of both nickel and copper was studied in single and binary systems using iron oxide Fe_2O_3 used as a nanomaterial, which show endothermic reactions with and thermodynamically favorable [38]. The determine ΔG for the copper binding were in the range of −19 to −21 kJ/mol, ΔH was 52.32 and ΔS was 250 J/mol K. Nickel has similar thermodynamic binding values which were as follows ΔG −22 to−27 kJ/mol, ΔH 45.75 and ΔS 230 J/molK. Further studies using MnO_2 for the removal of copper ions were performed and indicated that the binding was also endothermic [27].

The ΔH and ΔS were determined using the standard thermodynamic relationship. As shown in equation 3 below:

$$\Delta G = \Delta H - T\Delta S \quad (3)$$

Where ΔH is the enthalpy, ΔS is the entropy of the reaction, and T is the temperature in kelvin. By substituting equation 1 into equation 2 and with some rearrangement equation (4) can be developed. Equation 3 shows the relationship between the distribution coefficient ΔH, and ΔS:

$$LnK_d = \frac{\Delta S}{R} - \frac{\Delta H}{RT} \quad (4)$$

Where K_d is the distribution coefficient, ΔS is the entropy of the reaction, ΔH is the enthalpy of the reaction, R is the gas constant, and T is the temperature in Kelvin for the reaction. By plotting the LnK_d versus the 1/T, the slope of the line is the negative of the ΔH of the reaction divide by the gas constant. The intercept of the plot is the ΔS divided by the gas constant. ΔH gives an indication of the mechanism of the binding, when the ΔH value is below 40 kJ/mol the binding is through a chemisorption mechanism. Whereas ΔH values above 40 kJ/mol are indicative of physisorption. The ΔH from the present study indicates that the binding of both Cu^{2+} and Ni^{2+} to the SnO_2 nanomaterial was occurring through a chemisorption process, which corroborates the data determined through the activation studies. In addition, the data indicates that the binding for both Cu^{2+} and Ni^{2+} to the SnO_2 nanomaterial was an endothermic reaction both ΔH values were positive. The Cu^{2+} ions had a ΔH of binding approximately double that of the Ni^{2+} ions indicating the binding of Cu^{2+} is more endothermic than Ni^{2+}. Similarly the binding of As(III)/As(V), Cr(III)/Cr(VI), Co^{2+}, and Mn^{2+} have been found to bind to metal oxide nanomaterials through endothermic reactions [9, 53–55]. The results corroborate the data obtained from the Gibbs free energy studies indicating an endothermic reaction was occurring. The ΔS showed a positive value for the binding of both the Cu^{2+} and the Ni^{2+} to the SnO_2 nanomaterial. The results shown in Table 6 show that copper has a ΔS that is approximately double that of the Ni^{2+}, indicating that the binding of copper is more favorable than the Ni^{2+}. The higher ΔS for copper corroborates the capacity data, where it was observed that the binding capacity was higher than the Ni^{2+}. The higher ΔS value in binding could be related to the Cu^{2+} ions disturbing more of the water molecules bound to the SnO_2 nanomaterial than the Ni^{2+} to accommodate the binding. As well the disruption of the hydration sphere around the metal ions will also be important in determining the change in entropy. Many other metal ions including Cu^{2+} and Ni^{2+} bound to metal oxides have shown increases in the ΔS during the study of the thermodynamics of metal ion binding.

3.6 Interference

Figure 6a. and b. show the results of the interference studies that were performed at the optimum binding. The study was performed to investigate the effect of hard cations on the binding of both Cu^{2+} and Ni^{2+} that are commonly found in the water. In addition, the experiment was performed using a combination of all the cations in solution. More specifically, Figure 6a. shows the Ni^{2+} binding in the presence of the selected hard cations. The data shows that up to a concentration of all the cations in solution little to no effect on the binding was observed the binding was in the range of 85 to 100%. Above 30 ppm both Na^+ and K^+ showed little to no interference on the binding of Ni^{2+} ions. The Ni^{2+} in the presence of Ca^{2+}, Mg^{2+} and combined interference showed decreases up to approximately 50% of the binding, when compared to lower interference concentration. The decrease in binding observed in the presence of Ca^{2+}, Mg^{2+}, and the combined interferences indicates there is some competition in the binding at high concentrations. The competition in binding would be expected somewhat, for example in the combined interference solution there is a ratio of 26447:1 for the interference to Ni^{2+} ions. Even in such a high concentration of interfering ions there is still approximately 40% binding. This indicates that there is a preferential binding of the Ni^{2+} ions over the hard cations.

The binding of Cu^{2+} to the SnO_2 nanomaterial is shown in Figure 6B. As can be seen in Figure 6B, for the most part the binding of the Cu^{2+} ions to the SnO^2 in the presence of common hard cations is unaffected for the most part. The binding of the Cu^{2+} for the most part is above 90% even in the presence of 1000 ppm of each of the cations in one solution. The only cation that showed a negative effect on the binding of the Cu^{2+} ions was the Ca^{2+}, which showed approximately a 30% decrease in the binding at a Ca^{2+} concentration of 1000 ppm. However, in the combined interference solution this decrease in the binding was not observed, which is a mole ratio of 28663:1 interference to Cu^{2+}. This indicates that the interferences are not additive and there is some kind of synergistic effect observed, in the multi-element binding solution.

Similar results on the binding of cations to different nanomaterials in the presence of hard cations. For example Cu^{2+} binding to Fe_2O_3 and Fe_3O_4 nanomaterials in the presence of hard cations showed little to no interference on the binding [25]. In addition the binding of Pb^{2+} to Fe_2O_3 and Fe_3O_4 nanomaterials in the presence of similar hard cations showed little to no interference on the binding [25].

After 30 ppm is starts to vary however, all the cations do have an effect on the binding strain above 50%. However, there were a couple of that were below the strain of 50%. Magnesium at 300 ppm had a 30% strain and at 1000 ppm it had less than 20% strain. In previous interference studies used a different nanomaterial such as MnO_2 and the cations had a different percentage of binding with Ni^{2+} [22]. In previous studies of both Cu^{2+} and Ni^{2+} using the nano-particle shows that the certain cations had effect more than the others. [22] In figure 6b. Shows the data that obtain for the cations binding percentage with Cu^{2+}. All the cations from 0.3 ppm and 30 ppm all had a very high percentage of binding over 95%. This shows that all had a high binding are very synergistic.

4.0 Conclusion

SnO_2 was synthesized using a titration/precipitation method followed by calcination and was found to have an average grain size of 11.2 nm. The synthesized SnO_2 was successful in the removal of both Ni^{2+} and Cu^{2+}ions from aqueous solution. The optimum binding pH for both ions was determined to be pH 5 for both Ni^{2+} and Cu^{2+}. Binding capacities of the nanomaterial determined from the isotherm studies were comparable to numerous materials in the literature. The thermodynamic parameters for the binding of both the Cu^{2+} and Ni^{2+} ions showed and endothermic reaction as can be determined from the decreasing ΔG with increasing temperature as well as the positive ΔH values determined for both ions. The values for ΔH for Cu^{2+} binding was 28.73 kJ/mol and Nickel (II) was 13.37 KJ/mol. The negative values indicate that the binding of Copper (II) and Nickel (II) to the nanomaterial was endothermic. In addition, the kinetics for the binding were determined to be zeroth order. The activation energy studies indicate that the binding was occurring through chemisorption for both ions which had E_a for the binding process above 4 kJ/mol.

Acknowledgments

Authors would like to thank the NIH UTPA RISE program (Grant Number 1R25GM100866-03). The Department of Chemistry at the University of Texas Rio Grande Valley is grateful for the generous support provided by a Departmental Grant from the Robert A. Welch Foundation (Grant No. BX-0048).

References

1. Aziz HA, Adlan MN, Ariffin KS. Heavy metals (Cd, Pb, Zn, Ni, Cu and Cr(III)) removal from water in Malaysia: Post treatment by high quality limestone. Bioresource Technol. 2008; 99:1578–1583.
2. Gupta VK. Equilibrium Uptake, Sorption Dynamics, Process Development, and Column Operations for the Removal of Copper and Nickel from Aqueous Solution and Wastewater Using Activated Slag, a Low-Cost Adsorbent. Ind Eng Chem Res. 1998; 37:192–202.
3. Gayathri R, Kumar PS, Ramakrishnan K. Removal of Nickel (II) from aqueous solution by ceralite Ir 120 cationic exchange resins. Eng Sci Technol. 2010; 5:232–243.
4. Kurniawan TA, Chan GYS, Lo WH, Babel S. Physico–chemical treatment techniques for wastewater laden with heavy metals. Chem Eng. 2011; 118:83–98.
5. Jenkins D, Russell LL. Heavy Metals Contribution of Household Washing Products to Municipal Wastewater. Water Environ Fed. 1994; 66:805–813.
6. Agoubordea L, Naviab R. Heavy metals retention capacity of a non-conventional sorbent developed from a mixture of industrial and agricultural wastes. J Hazard Mater. 2009; 167:536–544. [PubMed: 19188023]
7. Dean GJ, Bosqul KH, Lanouette FL. Removing heavy - metals from waste water. Environ Sci Technol. 1972; 6:518–522.
8. Arbabi M, Golshani N. Removal of Copper Ions Cu (II) From Industrial Wastewater: A Review of Removal Methods. Int J Epidemiol Res. 2016; 3:283–293.
9. Yavuz O, Altunkaynak Y, Güzel F. Removal of copper, nickel, cobalt and manganese from aqueous solution by kaolinite. Water Res. 2003; 37(4):948–952. [PubMed: 12531278]
10. Mukherjee S, Kumar S, Misra AK, Acharya PC. Removal of aqueous nickel (II) using laterite as a low-cost adsorbent. Water Environ Res. 2006; 78:2268–2275. [PubMed: 17120446]
11. Vengris T, Binkiene R, Sveikauskaite A. Nickel, copper and zinc removal from waste water by a modified clay sorbent. Appl Clay Sci. 2001; 18:183–190.
12. Barakat MA. New trends in removing heavy metals from industrial wastewater. Arabian J Chem. 2011; 4:361–377.
13. Fu F, Wang Q. Removal of heavy metal ions from wastewaters: A review. J Environ Manage. 2011; 92:407–418. [PubMed: 21138785]
14. Forster CF, Quek SY, Wase DAJ. The Use of Sago Waste for the Sorption of Lead and Copper. Water SA. 1998; 24:251–256.
15. Kinniburgh DG, Jackson ML, Syers JK. Adsorption of Alkaline Earth, Transition, and Heavy Metal Cations by Hydrous Oxide Gels of Iron and Aluminum. Soil Sci Soc Am J. 1976:796–799.
16. Healy TW, James RO. Adsorption of Hydrolyzable Metal Ions at the Oxide—Water Interface. III. A Thermodynamic Model of Adsorption. J Colloid Interface Sci. 1972:65–81.
17. Dimitrova SV. Metal Sorption on Blast-Furnace Slag. Water Res. 1996:228–232.
18. Villaescusa I, Fiol N, Martínez M, Miralles N, Poch J, Serarols J. Removal of copper and nickel ions from aqueous solutions by grape stalks wastes. Water Res. 2004; 38(4):992–1002. [PubMed: 14769419]
19. Hua M, Zhang S, Pan B, Zhang W, Lv L, Zhang Q. Heavy Metal Removal From Water/Wastewater by Nanosized Metal Oxides: A Review. J Hazard Mater. 2011:317–331.
20. Das NC, Bandyopadhyay M. Water Environment Research. 1992; 64(7):852–857.
21. Akbal F, Camc S. Cooper, chromium and nickel removal from metal plating wastewater by electrocoagulation. Desalination. 2011; 269(1–3):214–222.

22. Sharma M, Choudhury D, Hazra SS, Basu S. Effective removal of metal ions from aqueous solution by mesoporous MnO_2 and TiO_2 monoliths: Kinetic and equilibrium modelling. J Alloys Compd. 2017; 720:221–229.
23. Dursun AY, Kalayci CS. Adsorption of Copper on Chitin-based materials: Kinetic and thermodynamic studies. J Taiwan Inst Chem Eng. 2016; 65:140–148.
24. Luther S, Borgfeld N, Kim JJ, Parsons G. Removal of arsenic from aqueous solution: A study of the effects of pH and interfering ions using iron oxide nanomaterialsCr(III)/Cr(VI) Fe_3O_4/Fe_2O_3. Microchem J. 2012; 101:30–36.
25. Tamez C, Hernandez R, Parsons JG. Removal of Cu (II) and Pb (II) from Aqueous Solution using engineered Iron Oxide Nanoparticles. Microchem J. 2016 Mar 1.125:97–104. [PubMed: 26811549]
26. Gonzalez CM, Hernandez J, Peralta-Videa JR, Botez CE, Parsons JG, Gardea-Torresdey JL. Sorption kinetic study of selenite and selenate onto a high and low pressure aged iron oxide nanomaterial. J Hazard Mater. 2012 Apr 15.0:138–145.
27. Han R, Zou W, Li H, Shi J. Copper(II) and lead(II) removal from aqueous solution in fixed-bed columns by manganese oxide coated zeolite. J Hazard Mater. 2006; 137(2):934–942. [PubMed: 16621258]
28. Rodríguez-Carvajal J. Recent advances in magnetic structure determination by neutron powder diffraction. Physica B. 1993; 192:55–69.
29. LeBail A, Duroy H, Fourquet JL. Mat Res Bull. 1988; 23:447.
30. Wang C, Zhou Y, Ge M, Xu X, Zhang Z, Jiang JZ. Large-Scale Synthesis of SnO_2 Nanosheets with High Lithium Storage Capacity. J Am Chem Soc. 2010; 132:46–47. [PubMed: 20000321]
31. Kosmulski M. pH-dependent surface charging and points of zero charge. IV. Update and new approach. J Colloid Interface Sci. 2009; 337:439–448. [PubMed: 19501839]
32. Pechenyuk SL. The use of the pH at the point of zero charge for characterizing the properties of oxide hydroxides. Russ Chem Bull. Jun.1999 48(6)
33. Parsons JG, Lopez ML, Peralta-Videa JR, Gardea-Torresdey JL. Determination of arsenic(III) and arsenic(V) binding to microwave assisted hydrothermal synthetically prepared Fe_3O_4, Mn_3O_4, and $MnFe_2O_4$ nanoadsorbents.
34. Ngomsika AF, Bee A, Siaugue JM, Cabuil V, Cote G. Nickel adsorption by magnetic alginate microcapsules containing an extractant. Water Res. 2006; 40:1848–1856. [PubMed: 16631227]
35. Nadaroglu H, Kalkan E, Demir N. Removal of copper from aqueous solution using red mud. Desalination. 2010; 251:90–95.
36. Mahapatra A, Mishra BG, Hota G. Electrospun Fe_2O_3–Al_2O_3 nanocomposite fibers as efficient adsorbent for removal of heavy metal ions from aqueous solution. J Hazard Mater. 2013; 258–259:116–123.
37. Sharma YC, Srivastava V, Upadhyay SN, Weng CH. Alumina Nanoparticles for the Removal of Ni(II) from Aqueous Solutions. Ind Eng Chem Res. 2008; 47:8095–8100.
38. Bouljelben N, Bouzid J, Elouear Z. Adsorption of nickel and copper onto natural iron oxide-coated sand from aqueous solutions: Study in single and binary systems. J Hazard Mater. 2009; 163(1): 376–382. [PubMed: 18701213]
39. Aydn H, Bulut Y, Yerlikaya C. Removal of copper (II) from aqueous solution by adsorption onto low-cost adsorbents. J Environ Manage. 2008; 87:37–45. [PubMed: 17349732]
40. Cho DW, Jeon BH, Chon CM, Kim Y, Schwartz FW, Lee ES, Song H. A novel chitosan/clay/magnetite composite for adsorption of Cu(II) and As(V). Chem Eng J. 2012; 200–202:654–662.
41. Sprynskyy M, Buszewski B, Terzyk APJ. Namiesnik Study of the selection mechanism of heavy metal (Pb^{2+}, Cu^{2+}, Ni^{2+}, and Cd^{2+}) adsorption on clinoptilolite. J Colloid Interface Sci. 2006; 304:21–28. [PubMed: 16989853]
42. Demirbas E, Dizge N, Sulak MT, Kobya M. Adsorption kinetics and equilibrium of copper from aqueous solutions using hazelnut shell activated carbon. Chem Eng J. 2009; 148:480–487.
43. Fouladgar M, Beheshti M, Sabzyan H. Single and binary adsorption of nickel and copper from aqueous solutions by γ-alumina nanoparticles: Equilibrium and kinetic modeling. J Mol Liq. 2015; 211:1060–1073.

44. Heidari A, Younesi H, Mehraban Z, Heikkinen H. Selective adsorption of Pb(II), Cd(II), and Ni(II) ions from aqueous solution using chitosan–MAA nanoparticles. Int J Biol Macromol. 2013; 61:251–263. [PubMed: 23817093]
45. Ghaee A, Shariaty-Niassarb M, Barzin J, Zarghan A. Adsorption of copper and nickel ions on macroporous chitosan membrane: Equilibrium study. Appl Surface Sci. 2012; 258:7732–7743.
46. Bayat B. Comparative study of adsorption properties of Turkish fly ashes I. The case of nickel(II), copper(II) and zinc(II). J Hazard Mater. 2002; 95:251–273. [PubMed: 12423941]
47. Wang S, Soudi M, Li L, Zhu ZH. Coal ash conversion into effective adsorbents for removal of heavy metals and dyes from wastewater. J Hazard Mater. 2006; 133:243–251. [PubMed: 16310947]
48. Gao Z, Bandosz TJ, Zhao Z, Han M, Qiu J. Investigation of factors affecting adsorption of transition metals on oxidized carbon nanotubes. J Hazard Mater. 2009; 167:357–365. [PubMed: 19264402]
49. Phuengprasop T, Sittiwong J, Unob F. Removal of heavy metal ions by iron oxide coated sewage sludge. J Hazard Mater. 2011; 186:502–507. [PubMed: 21167637]
50. Gupta VK, Ali I. Utilization of bagasse fly ash (a sugar industry waste) for the removal of copper and zinc from wastewater. Sep Purif Technol. 2000; 18:131–140.
51. Chen C, Wang X. Adsorption of Ni(II) from Aqueous Solution Using Oxidized Multiwall Carbon Nanotubes. Ind Eng Chem Res. 2006; 45:9144–9149.
52. Panneerselvam P, Morad N, Tan KA. Magnetic nanoparticle (Fe_3O_4) impregnated onto tea waste for the removal of nickel(II) from aqueous solution. J Hazard Mater. 2011; 186:160–168. [PubMed: 21146294]
53. Cantu Y, Remes A, Reyna A, Martinez D, Villarreal J, Ramos H, Trevino S, Tamez C, Martinez A, Eubanks T, Parsons JG. Thermodynamics, kinetics, and activation energy studies of the sorption of chromium(III) and chromium(VI) to a Mn_3O_4 nanomaterial. Chem Eng J. 2014; 254:374–3834. [PubMed: 25097453]
54. Luther S, Brogfeld N, Kim J, Parsons JG. Study of the thermodynamics of chromium(III) and chromium(VI) binding to iron(II/III)oxide or magnetite or ferrite and manganese(II) iron (III) oxide or jacobsite or manganese ferrite nanoparticles. J Colloid and Interface Sci. 2013; 400:97–103. [PubMed: 23558081]
55. Rajurkar NS, Gokarn AN, Dimya K. Adsorption of Chromium(III), Nickel(II), and Copper(II) from Aqueous Solution by Activated Alumina. Clean – Soil, Air, Water. 2011; 39:767–773.

Highlights

- A SnO_2 nanomaterial was synthesized through a precipitation-calcination process from $SnCl_4$ in aqueous solution
- The binding of both Cu^{2+} and Ni^{2+}ions from aqueous solution to the SnO_2 nonmaterial were tested
- The Binding parameters investigated included pH, kinetics (time dependency), and thermodynamics
- Hard cations showed little to no effect on the binding of either cation ions to the SnO_2 nanomaterial

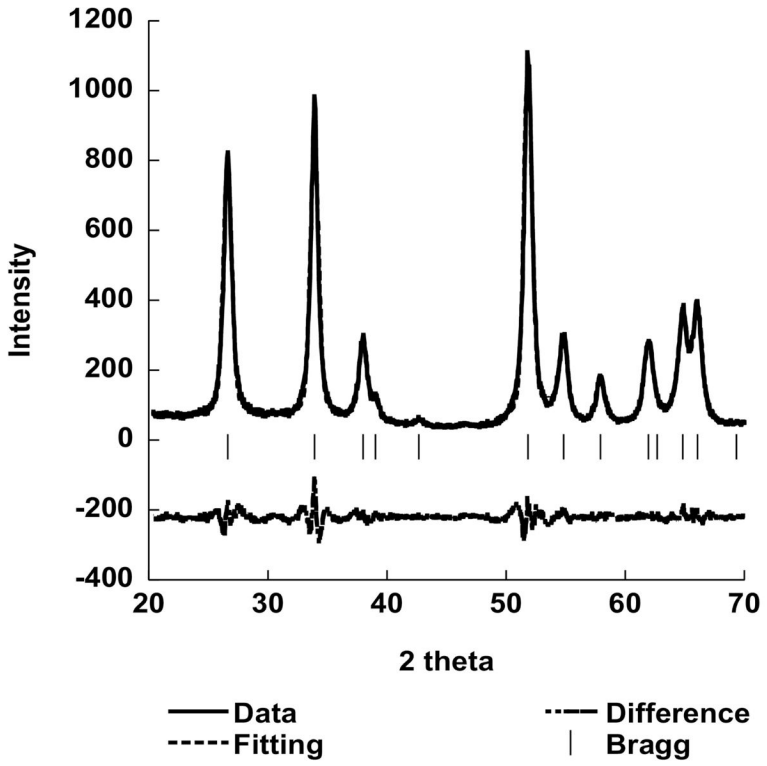

Figure 1.

XRD pattern of the synthesized SnO_2 nanomaterial and LeBail fitting of the collected from 20 to 60° in 2θ.

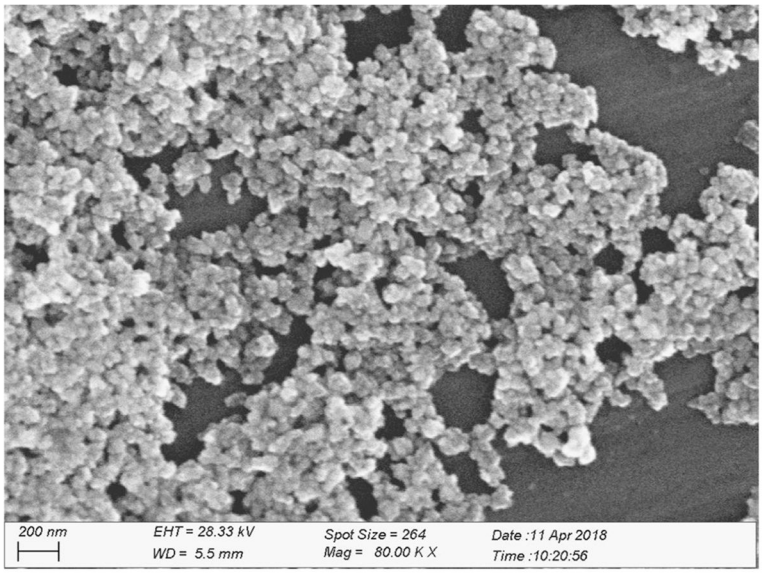

Figure 2.
SEM image of the synthesized SnO_2 nanoparticles.

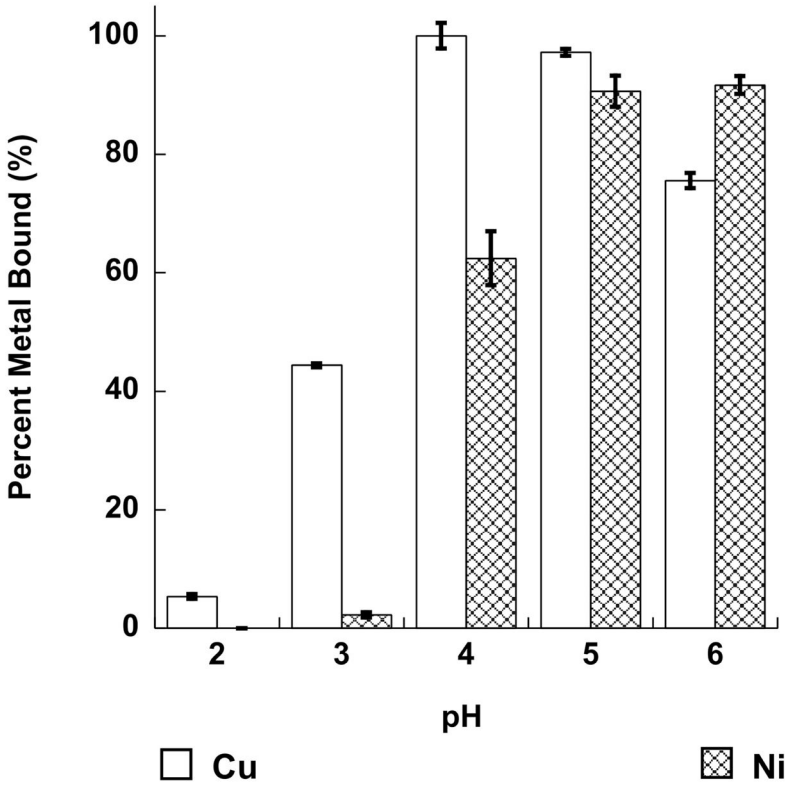

Figure 3.

pH profile for the binding of Cu^{2+} and Ni^{2+} ions to the synthesized SnO_2 nanoparticles from pH 2 through pH 6.

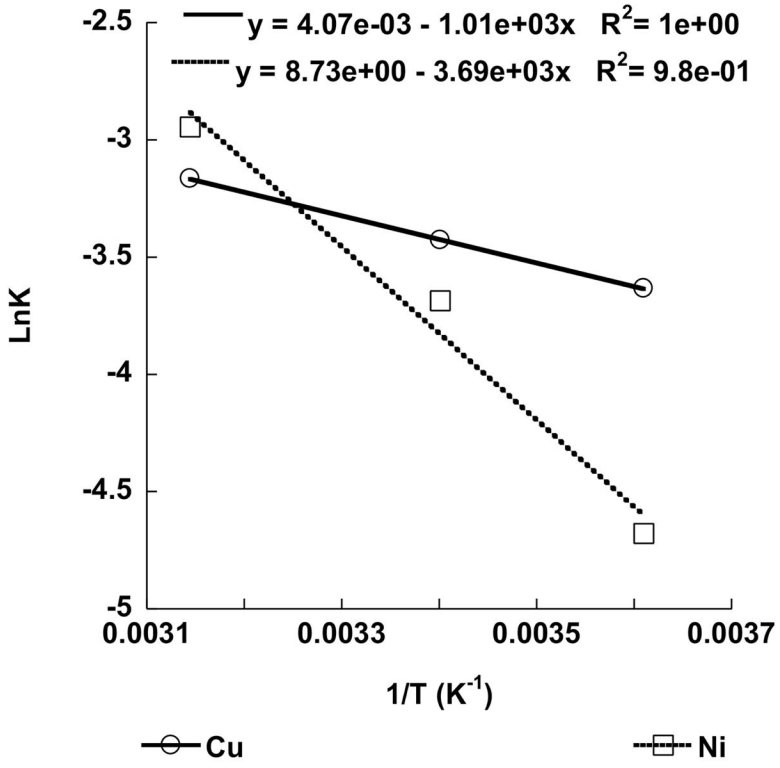

Figure 4.

Arrhenius plot for the binding of Cu^{2+} and Ni^{2+} ions to SnO_2 nanoparticles at temperatures of 4, 21, and 45 °C

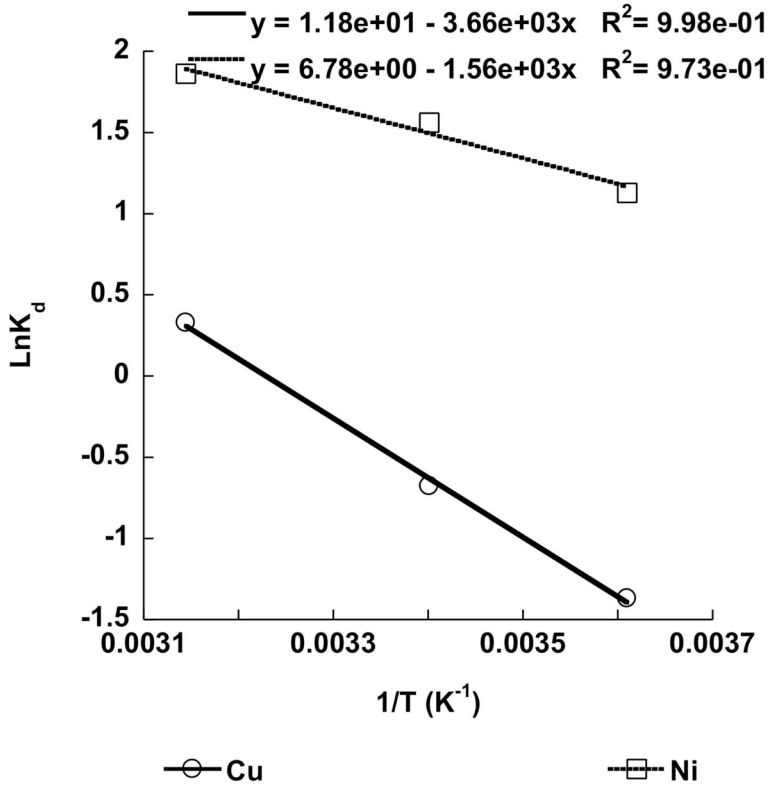

Figure 5.

Thermodynamic plot for the binding of Cu^{2+} and Ni^{2+} ions to the synthesized SnO_2 nanoparticles at temperatures of 4, 21, and 45 °C.

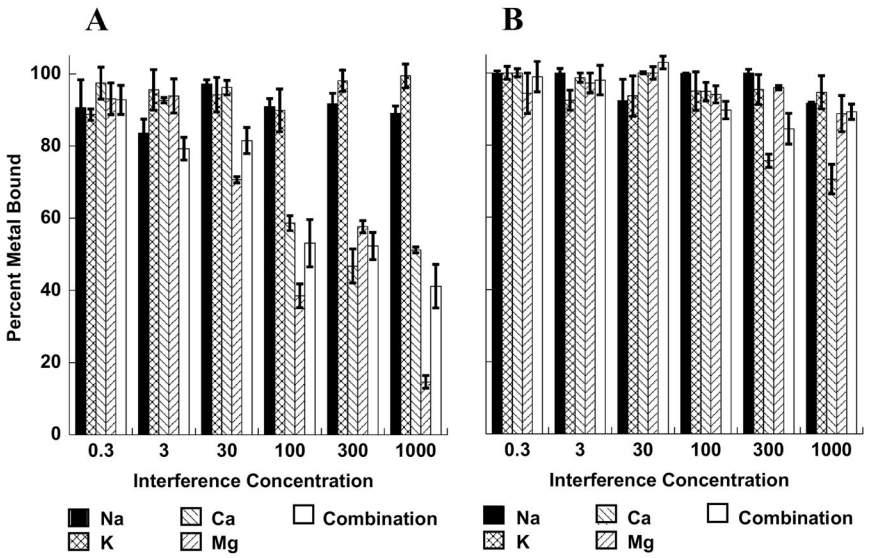

Figure 6.

Interference of hard cations on the binding of Ni (**A**) and Cu (**B**) to the synthesized SnO_2 nanoparticles at the optimum binding pH.

Table 1

Operating parameters for the Perkin Elmer PinAAcle 900 GFAAS for copper analysis

Parameter	Temperature (°C)	Ramp Time (s)	Hold Time (s)
Pre-Dry	110	1	30
Dry	130	15	30
Char	1200	10	20
Atomization	2000	0	5
Clean out	2400	1	2

Table 2

Operating parameters for the Perkin Elmer PinAAcle 900 GFAAS for nickel analysis

Parameter	Temperature (°C)	Ramp Time (s)	Hold Time (s)
Pre-Dry	110	1	30
Dry	130	15	30
Char	1200	10	20
Atomization	2000	0	5
Clean out	2400	1	2

Table 3

Operating parameters for the Perkin Elmer 8300 DV ICP-OES for copper and nickel analysis

Parameter	Setting
λ_{Cu}	327.393 nm
λ_{Ni}	231.604 nm
RF power	1500 w
Nebulizer	Gemcone (low Flow)
Plasma Flow	15 L/min
Auxiliary Flow	0.2L/min
Nebulizer Flow	0.55 mL/min
Sample flow	1.50 mL/min
Injector	2.0 mm Alumina
Spray Chamber	Cyclonic
Integration Time	20 s
Replicates	3

Table 4

Binding capacities for the Cu^{2+} and Ni^{2+} sorption to the SnO_2 nanoparticles at of 4, 21, and 45 °C.

Ion	Temperature (°C)	Capacity (mg/g)	Capacity (mol/g)
Cu^{2+}	4	2.63	0.041
	21	2.95	0.046
	45	3.27	0.051
Ni^{2+}	4	0.79	0.014
	21	1.07	0.018
	45	1.46	0.025

Table 5

Adsorption capacities for the binding of Cu^{2+} and Ni^{2+} to various materials and nanomaterials from the literature.

Ion	Material	Capacity (mg/g)	Capacity (mmol/g)	Ref.
Cu^{2+}	Kaolinite	1.669	0.026	[9]
Ni^{2+}	Kaolinite	10.787	0.17	[9]
Cu^{2+}	iron oxide-coated sand	2.04	0.032	[27]
Ni^{2+}	iron oxide-coated sand	0.28	0.0048	[27]
Ni^{2+}	magnetic alginate microcapsules	33.04	0.52	[34]
Cu^{2+}	Red Mud	5.439	0.09	[35]
Cu^{2+}	Electrospun Fe_2O_3–Al_2O_3 nano-fibers	4.98	0.078	[36]
Ni^{2+}	Electrospun Fe_2O_3–Al_2O_3 nano-fibers	32.36	0.55	[36]
Ni^{2+}	Alumina Nanoparticle	30.0	0.51	[37]
Cu^{2+}	chitosan/clay/magnetite	14.3	0.23	[40]
Cu^{2+}	clinoptilolite	25.69	0.40	[41]
Ni^{2+}	clinoptilolite	15.55	0.26	[41]
Cu^{2+}	Lentil Shells	8.997	0.14	[42]
Cu^{2+}	Wheat Shells	9.510	0.15	[42]
Cu^{2+}	Rice Shells	9.588	0.15	[42]
Cu^{2+}	Activated C (hazelnut shells)	58.27	0.92	[42]
Cu^{2+}	Activated C (Pecan Shell)	95.00	1.49	[42]
Cu^{2+}	Activated Carbon (Peacan Hull)	65.57	1.031	[42]
Cu^{2+}	Carbon (Sawdust)	5.73	0.090	[42]
Cu^{2+}	γ-alumina nanoparticles	51.3	0.81	[43]
Ni^{2+}	γ-alumina nanoparticles	238.1	4.06	[43]
Cu^{2+}	Magnetic chitosan nanoparticles	35.5	0.56	[44]
Ni^{2+}	chitosan–MAA nanoparticles	1.13	0.019	[44]
Cu^{2+}	chitosan membrane	25.64	0.40	[45]
Ni^{2+}	chitosan membrane	10.30	0.18	[45]
Cu^{2+}	Fly Ash	1.351	0.021	[46]
Ni^{2+}	Fly Ash	0.480	0.0082	[46]
Cu^{2+}	Fly Ash	1.554	0.024	[46]
Ni^{2+}	Fly Ash	0.124	0.0021	[46]
Cu^{2+}	Coal Ash	42	0.66	[47]
Ni^{2+}	Coal Ash	28	0.447	[47]
Cu^{2+}	Oxidized carbon nanotubes	2.57	0.0404	[48]
Ni^{2+}	Oxidized carbon nanotubes	1.82	0.0311	[48]
Cu^{2+}	Iron oxide coated sewage sludge	17.3	0.27	[49]
Ni^{2+}	Iron oxide coated sewage sludge	7.8	0.13	[49]

Ion	Material	Capacity (mg/g)	Capacity (mmol/g)	Ref.
Cu^{2+}	bagasse fly ash	2.26	0.036	[50]
Ni^{2+}	Oxidized Multiwall Carbon Nanotubes	8.77	0.15	[51]
Ni^{2+}	Magnetic Nanoparticles (Fe)	11.53	0.20	[52]

Table 6

Kinetics data for the binding of Cu^{2+} and Ni^{2+} to the SnO_2 nanoparticles at temperatures of 4, 21, and 45 °C.

Ion	Temperature (°C)	Slope	R^2
Cu^{2+}	4	0.0264	0.99
	21	0.0325	0.99
	45	0.0422	0.99
Ni^{2+}	4	0.0093	0.98
	21	0.0251	0.98
	45	0.0526	0.98

Table 7

Thermodynamic parameters for the binding of Cu^{2+} and Ni^{2+} to the SnO_2 nanoparticles at of 4, 21, and 45 °C.

Ion	Temperature (°C)	ΔG (kJ/mol)	ΔH (kJ/mol)	ΔS (J/mol)	Ea(kJ)
Cu^{2+}	4	3.13			13.99
	21	1.66	28.73	92.65	
	45	−0.86			
Ni^{2+}	4	−2.85			8.09
	21	−3.83	13.37	54.53	
	45	−4.91			